Electron acceleration in intense laser – solid interactions at parallel incidence

X.F. Shen, A.M. Pukhov, S.E. Perevalov, A.A. Soloviev

Abstract. **Using multidimensional particle-in-cell simulations, we show that an electron beam with a huge space charge can be accelerated to high energies by irradiating the edge of a solid density target with an intense femtosecond laser pulse at parallel incidence. The process of energy gain of each electron is divided into two parts: the transverse laser field and the longitudinal field of the excited surface plasma wave (SPW). It is shown that the longitudinal field of the SPW dominates the acceleration of the major part of electrons. This process leads to generation of a highly collimated electron beam with a huge space charge.**

1. Introduction

One of the most promising applications of intense laser-plasma interaction is the generation of high-energy electron beams. Since 1979, various acceleration mechanisms have been proposed and demonstrated that work at different laser and plasma parameters [1–6]. Recently, the interaction of laser radiation with structural targets has been intensively studied, including hollow tubes, arrays of nano- and microwires, slabs and other similar configurations [7–17]. In these regimes, the laser energy is coupled into transverse magnetic modes {we call it surface plasma wave (SPW) [18] hereinafter}. The laser pulse is actually incident parallel to the lateral surfaces of the target, different from the normal or oblique incidence used in typical laser planar target interactions [19–21]. At parallel incidence a significant amount of electrons can be peeled off from the skin-layer of the target and accelerated along the lateral surface to high energies (we refer to this regime as the laser peeler regime). Two groups of electrons are distinguished. One is mainly accelerated by the laser transverse field, similar to the mechanism discussed in Ref. [22]. The other is dominated by the longitudinal field of the SPW [7, 8, 15, 16].

X.F. Shen, A.M. Pukhov Institut für Theoretische Physik I Heinrich-Heine-Universität Düsseldorf, Universitätsstraße 1, 40225 Düsseldorf, Germany; e-mail: shenx@uni-duesseldorf.de, pukhov@tp1.hhu.de;
S.E. Perevalov, A.A. Soloviev Institute of Applied Physics, Russian Academy of Sciences, ul. Ulyanova 46, 603950 Nizhny Novgorod, Russia; e-mail: perevalov@ipfran.ru

In the present paper, we explore the electron acceleration in the interaction of intense femtosecond laser pulses with solid targets ($n_e > 10^{23}$ cm^{-3}) at parallel incidence regime (laser peeler), where preplasmas covering the target around are considered. We find that the SPW-driven acceleration (SPWA) is the dominant acceleration mechanism and the maximum energy gain from the SPWA is about three times higher than that from the transverse acceleration. The accelerated electron beam is highly collimated with a space charge up to tens of nanocoulombs.

2. Simulation setup

The two-dimensional (2D) particle-in-cell (PIC) simulations are conducted with the EPOCH code [23] and the VLPL (Virtual Laser Plasma Lab) code [24]. A y-polarised laser pulse with an intensity of $I_0 = 2.16 \times 10^{20}$ W cm^{-2} and a wavelength of $\lambda = 800$ nm is focused on the front edge of a tape target. The laser field amplitude corresponds to a normalised vector potential $a_0 = E_{las}/E_0 = 10$, where E_{las} is the amplitude of the laser electric field; $E_0 = mc\omega_0/e$; ω_0 is the laser frequency; and m and e are the electron mass and charge, respectively. The laser beam has a temporal cosine profile with a FWHM duration $T_0 = 11$ fs. A transverse plane wave is used to clearly show the electron dynamics. The main target has a uniform solid density $n_e = 200n_{cr}$ (about 3.5×10^{23} cm^{-3}). Here $n_{cr} = m_e\omega_0^2/(4\pi e^2)$ is the critical density of electrons. The transverse thickness is 1.2λ and the longitudinal length is 80λ. Preplasmas cover the tape target around. In front of the edge, a linear density ramp with a scale length of 5λ is simulated, while in the lateral surfaces, the scale length is 0.5λ.

The simulation box is $12\lambda \times 40\lambda$ sampled by 2400×4000 cells, respectively, in the $x \times y$ directions. Each cell contains 100 macroparticles. A moving window is used to save computational resources. In the transverse direction, periodic boundary conditions are used for fields and open conditions are used for particles. In the EPOCH code, the algorithm proposed by Pukhov is used to minimise the numerical dispersion [24].

3. Simulation results and discussion

Figure 1 illustrates the formation process of an electron nanobunch. At the beginning ($t = 3.5T_0$), electrons are pushed forward by the laser ponderomotive force, forming a high density electron sheet in front of the edge that can excite a strong SPW (Figs 1a and 1e). Here $t = 0$ corresponds to the time when the laser pulse enters the simulation box. For a linearly polarised laser pulse, the ponderomotive force oscillates at twice the laser frequency. When it changes the sign, part of

electrons are pulled backward, while they are also accelerated upward by the laser electric field E_y (Figs 1g and h). Due to the transverse ponderomotive force, these electrons are compressed to a higher density, forming a dense electron nanobunch (Figs 1d and i). Subsequently, this nanobunch is accelerated forward by both the longitudinal field of the SPW and the laser transverse field (Figs 1e and j). This process looks like the nanobunch is 'peeled' off from the target surface by the laser pulse and it repeats every half a laser cycle, forming a series of electron nanobunches that are periodically distributed and separated by one laser wavelength on each side of the target (see Fig. 2c).

The simulation results at $t = 16T_0$ are shown in Fig. 2, which illustrates the distributions of the laser electric field E_y, the longitudinal electric field E_x of the SPW and the electron density n_e. Note that the field E_x near the thin film is the 'pure' SPW field, because the longitudinal field of the symmetric laser pulse is here equal to zero. One can clearly see that the SPW travels forward with the laser pulse with velocity close to the light speed. Meanwhile, the electron nanobunches are trapped inside the potential well of the SPW, which means they will gain energies directly from the longitudinal field of the SPW. To make this more clear, we present the energy-gain plane (W_x, W_y) of each electron at the moment of time $t = 80T_0$ (see Fig. 3), where W_x and W_y are defined as

$$W_x = -\int ev_x E_x \mathrm{d}t,$$

$$W_y = -\int ev_y E_y \mathrm{d}t.$$

The purple dashed line means that $W_x + W_y = 0$ and therefore all electrons are located in the upper right half-plane. The red dashed lines enclose areas preferably by the longitudinal and transverse acceleration, respectively. One can clearly see that most electrons gain more energy from the longitudinal field, that is, via the SPWA. For the most energetic electrons, the transverse field E_y even decelerates them ($W_y < 0$). The maximum value of W_x reaches about $\sim 450 m_e c^2$, which is about three times larger than that of W_y. This indicates that the SPW dominates the electron acceleration process in our regime.

In the following, we divide the electrons into two groups to facilitate our comparison and show their differences. Group A represents those electrons that gained more energy from the longitudinal component of the electric field, that is, $W_x > W_y$. Group B represents those electrons that gained more energy from the transverse component, that is, $W_x < W_y$.

The trajectories of representative electrons from groups A and B are shown in Figs 4a and 4b, respectively, where the trajectories are colour coded with respect to the relativistic electron energy γ. In Fig. 4a, electrons are selected from those satisfying the conditions $W_x > W_y$ and $W_x > 0.95 W_{x \max}$ at $t = 80T_0$, since we are mainly interested in high energy electrons (here $W_{x \max}$ is the maximum value of W_x at the considered moment of time). One can clearly see that these electrons are mainly accelerated forward close to the target surface, while the transverse displacements are very small. This is quite different from the electrons from group B. As shown in Fig. 4b, they have much larger transverse displacements while moving forward, since they are predominantly accelerated by the field E_y, and then turn forward by the $\boldsymbol{v} \times \boldsymbol{B}$ force. Meanwhile,

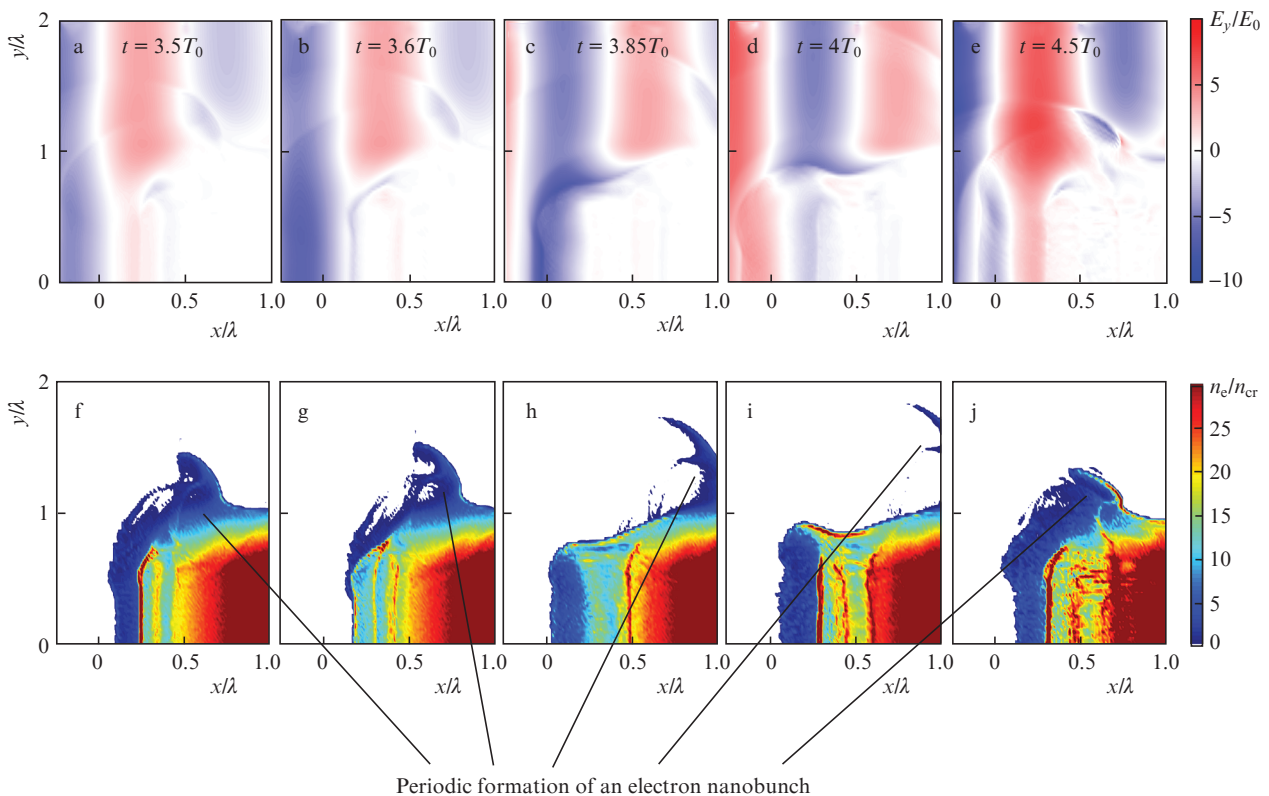Periodic formation of an electron nanobunch

Figure 1. (Colour online) (a–e) Temporal evolutions of the normalised laser transverse electric field E_y/E_0 and (f–j) electron density distributions n_e/n_{cr} at $t =$ (a, f) $3.5T_0$, (b, g) $3.6T_0$, (c, h) $3.85T_0$, (d, i) $4.0T_0$, and (e, j) $4.5T_0$, which illustrate the formation process of a dense electron nanobunch.
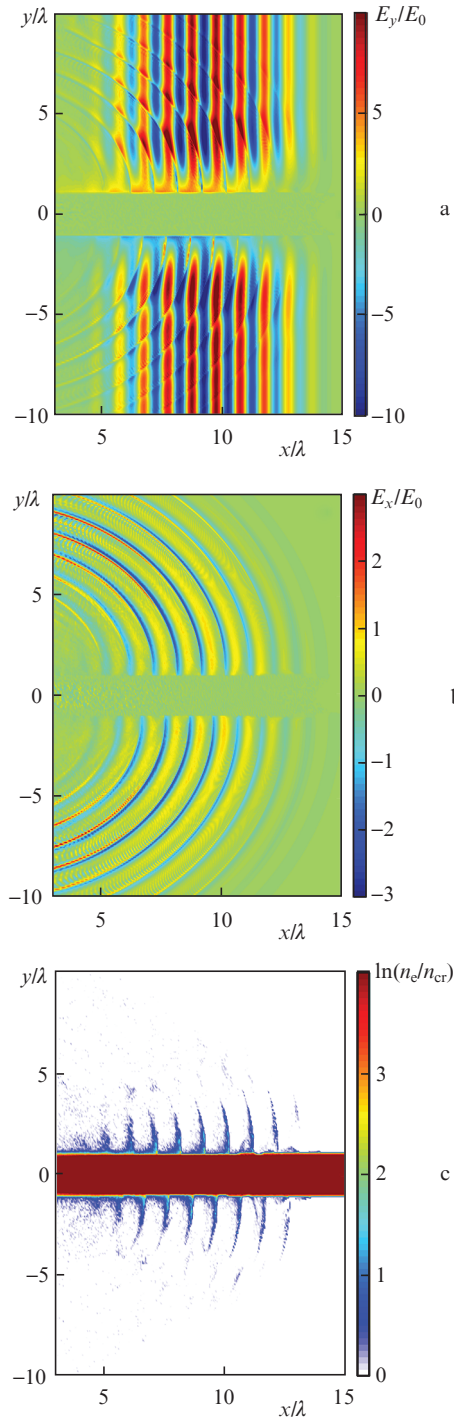
Figure 3. (Colour online) Energy-gain plane (W_x, W_y). The red dashed lines indicate the populations arising from the longitudinal (large W_x) and transverse (large W_y) acceleration. The purple dashed line corresponds to $W_x + W_y = 0$.

Figure 2. (Colour online) (a) Distributions of the normalised laser transverse electric field E_y/E_0, (b) the longitudinal component of the electric field E_x/E_0 and (c) the logarithmic colour scale of the electron density $\ln(n_e/n_{cr})$ at $t = 16T_0$.

these electrons oscillate transversely, which indicates that they slip into the accelerating or decelerating phase determined by their relative longitudinal positions with respect to the laser phase, similar to the acceleration process of a single electron in vacuum. However, due to the longitudinal component of the fields, they may achieve higher energies than the 'free electron' limit energy of $m_e c^2 a_0^2/2 \sim 26$ MeV [22]. Note that the representative electrons of group **B** are selected from those satisfying the conditions $W_x < W_y$ and $W_y > 0.85 W_{y\,\mathrm{max}}$,
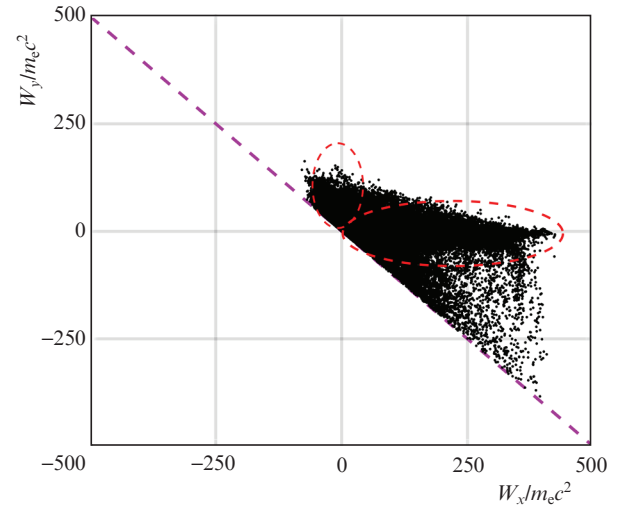
considering there are much fewer high energy electrons in this group. Here $W_{y\,\mathrm{max}}$ represents the maximum value of W_y at $t = 80T_0$.

The angular distributions of the two groups are presented in Fig. 5. For group A, the angular spread of electrons is extremely small; the divergence angle of the high-energy electrons (> 100 MeV) is only about 1° (Fig. 5a). Compared to this, the angular spread of electrons from group **B** is moderately larger, where the divergence angle is about 5° for those with energies larger than 50 MeV (Fig. 5b).

Figure 6a shows the temporal evolutions of the maximum electron energy E_{max}, $W_{x\,\mathrm{max}}$ and $W_{y\,\mathrm{max}}$. One can see that at the beginning these values increase faster and then approach saturation. The maximum energy at $t = 80T_0$ reaches about
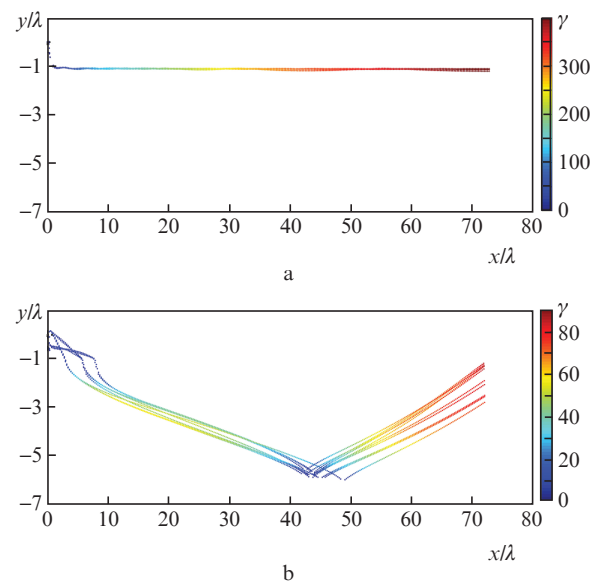

Figure 4. (Colour online) Trajectories of ten representative electrons from (a) group A and (b) group B, which are colour coded with respect to the relativistic electron energy γ.
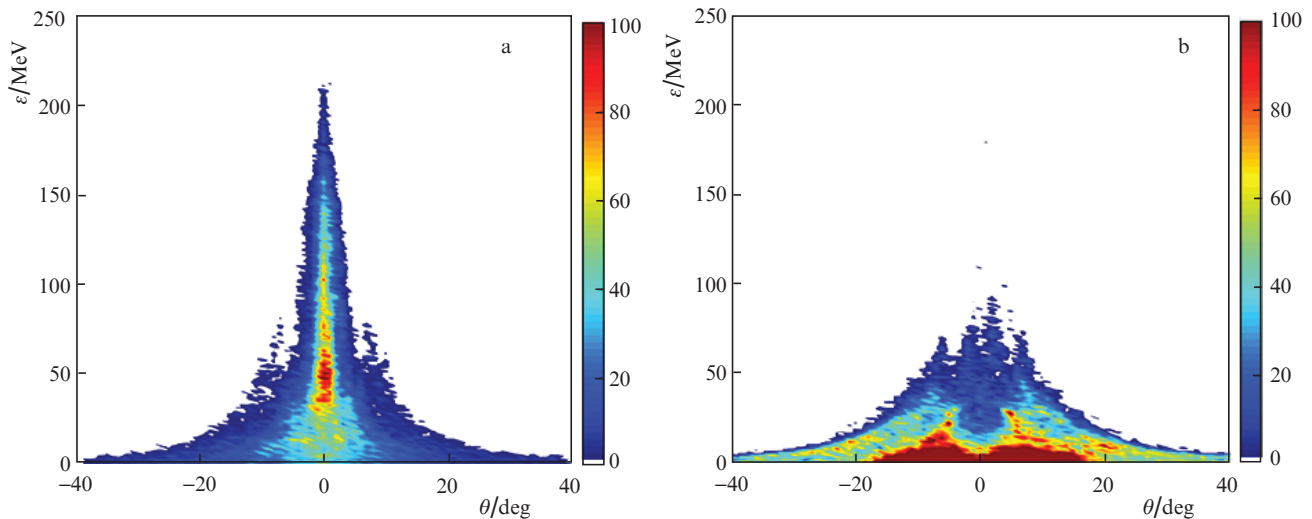
Figure 5. (Colour online) Angular distributions of electrons from (a) group A and (b) group B at $t = 80T_0$ (the colour scale represents the relative number of electrons).

220 MeV, which is much higher than the 'free electron' limit of 26 MeV. Note that here the the value of $W_{x\,max}$ is always slightly larger than that of E_{max}, which means that the transverse field even decelerates these electrons. The corresponding energy spectra are shown in Fig. 6b. One can see that most of high energy electrons are mainly accelerated by the longitudinal field, while only a small fraction predominantly comes from the transverse acceleration. The maximum electron energy in group B is about 90 MeV, much smaller than that in group A.

The total number of electrons with $\gamma > 10$ reaches about 7.5×10^{10}, while the number from groups A and B is about 5.4×10^{10} and 2.1×10^{10}, respectively. Here we take the length of the third dimension as 10λ.

4. Conclusions

Thus, using 2D PIC simulations, we investigated the electron acceleration in the solid peeler regime with preplasmas taken

into account. It is shown that the acceleration mainly comes from the longitudinal direction, that is, via the SPWA, leading to a highly collimated electron beam. The maximum electron energy reaches about 220 MeV that is much higher than the 'free electron' limit, and the space charge of high energy electrons can reach tens of nC, which is very important for relevant applications [10, 12, 16, 17, 25].
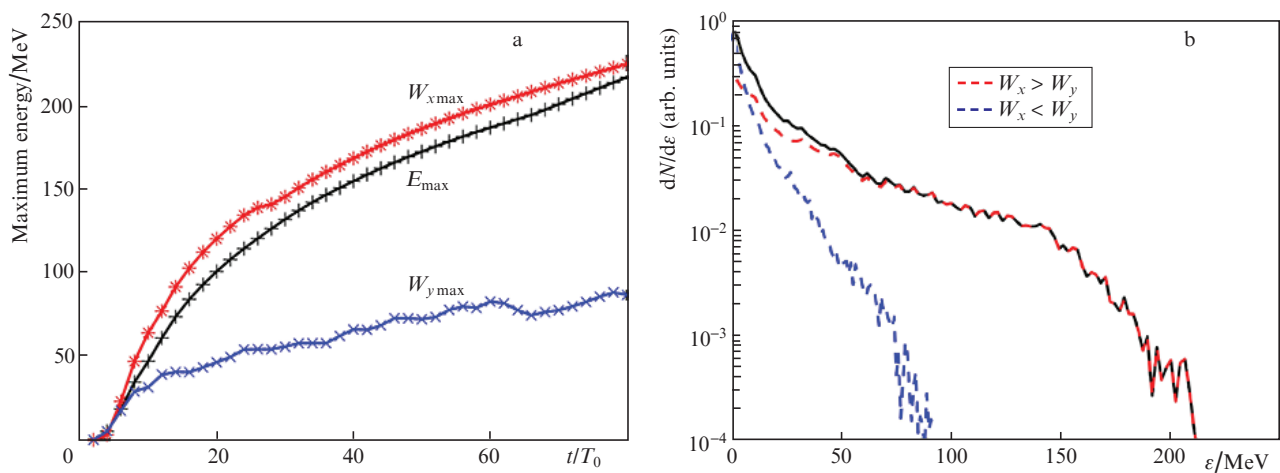
Figure 6. Colour online) (a) Temporal evolutions of the maximum electron energy E_{max} (black pluses), $W_{x\,max}$ (red asterisks) and $W_{y\,max}$ (blue crosses), as well as (b) energy spectra of all the electrons (black solid), electrons from group A (red dashed) and group B (blue dashed) at $t = 80T_0$.

References

1. Tajima T., Dawson J.M. *Phys. Rev. Lett.*, **43**, 267 (1979).
2. Pukhov A., Sheng Z.-M., Meyer-Ter-Vehn J. *Phys. Plasmas*, **6**, 2847 (1999).
3. Pukhov A., Meyer-Ter-Vehn J. *Appl. Phys. B*, **74**, 355 (2002).
4. Esarey E., Schroeder C.B., Leemans W.P. *Rev. Mod. Phys.*, **81**, 1229 (2009).
5. Gonsalves A.J., Gonsalves A.J., Nakamura K., Daniels J., Benedetti C., Pieronek C., De Raadt T.C.H., Steinke S., Bin J.H., Bulanov S.S., Van Tilborg J., Geddes C.G.R., Schroeder C.B., Tóth C., Esarey E., Swanson K., Fan-Chiang L., Leemans W.P., Bagdasarov G., Bobrova N., Gasilov V., Sasorov P., Korn G. *Phys. Rev. Lett.*, **122**, 084801 (2019).
6. Rosmej O.N., Günther M.M., Neumayer P., Zähter S., Gyrdymov M., Tavana P., Zahn N., Andreev N.E., Popov V.S., Borisenko N.G., Kantsyrev A., Skobliakov A., Panyushkin V., Bogdanov A., Consoli F., Shen X.F., Pukhov A. *Plasma Phys. Controlled Fusion*, **62**, 115024 (2020).
7. Kluge T., Gaillard S.A., Flippo K.A., Burris-Mog T., Enghardt W., Gall B., Geissel M., Helm A., Kraft S.D., Lockard T., Metzkes J., Offermann D.T., Schollmeier M., Schramm U., Zeil K., Bussmann M., Cowan T.E. *New J. Phys.*, **14**, 023038 (2012).
8. Xiao K.D., Huang T.W., Ju L.B., Yang S.L., Yang Y.C., Qiao B., Zhou C.T., He X.T., Ju L.B., Wu S.Z., Zhang H., Ruan S.C. *Phys. Rev. E*, **93**, 043207 (2016).
9. Kaymak V., Pukhov A., Shlyaptsev V.N., Rocca J.J. *Phys. Rev. Lett.*, **117**, 035004 (2016).
10. Yi L.Q., Pukhov A., Luu-Thanh P., Shen B. *Phys. Rev. Lett.*, **116**, 115001 (2016).
11. Jiang S., Ji L.L., George K.M., Snyder J., Krygier A., Poole P., Willis C., Daskalova R., Chowdhury E., Schumacher D.W., Freeman R.R., Akli K.U., Audesirk H., Lewis N.S., Pukhov A.. *Phys. Rev. Lett.*, **116**, 085002 (2016).
12. Zou D.B., Pukhov A.,Yi L.Q., Zhuo H.B., Yu T.P.,Yin Y., Shao F.Q. *Sci. Rep.*, **7**, 42666 (2017).
13. Curtis A., Hollinger R., Wang S., Wang Y., Shlyaptsev V.N., Rocca J.J., Calvi C., Rockwood A., Tinsley J., Kaymak V., Pukhov A. *Nat. Commun.*, **9**, 1077 (2018).
14. He H., Pei W.B., Fu S.Z., Qiao B., Shen X.F., Yao W.P., Xie Y., Zhou C.T., He X.T., Zhu S.P. *New J. Phys.*, **21**, 033035 (2019).
15. Gong Z., Robinson A.P.L., Yan X.Q., Arefiev A.V. *Plasma Phys. Controlled Fusion*, **61**, 035012 (2019).
16. Shen X.F., Pukhov A., Qiao B. arXiv:2009.04279 (2020).
17. Gizzi L.A. et al. *Phys. Rev. Research*, **2**, 033451 (2020).
18. Macchi A. *Phys. Plasma*, **25**, 031906 (2018).
19. Macchi A., Borghesi M., Passoni M. *Rev. Mod. Phys.*, **85**, 751 (2013).
20. Shen X.F., Qiao B., Zhang H., Kar S., Zhou C.T., Chang H.X., Borghesi M., He X.T. *Phys. Rev. Lett.*, **118**, 204802 (2017).
21. Qiao B., Shen X.F., He H., Xie Y., Zhang H., Zhou C.T., Zhu S.P., He X.T. *Plasma Phys. Controlled Fusion*, **61**, 014039 (2019).
22. Robinson A.P.L., Arefiev A.V., Neely D. *Phys. Rev. Lett.*, **111**, 065002 (2013).
23. Arber T., Bennett K., Brady C.S., Lawrence-Douglas A., Ramsay M.G., Sircombe N.J., Gillies P., Evans R.G., Schmitz H., Bell A.R., Ridgers C.P. *Plasma Phys. Controlled Fusion*, **57**, 113001 (2015).
24. Pukhov A. *J. Comput. Phys.*, **418**, 109622 (2020).
25. Shen X.F., Pukhov A., Günther M.M., Rosmej O.N. *Appl. Phys. Lett.*, **118**, 134102 (2021).